ACADEMIC PRESS

Available online at www.sciencedirect.com

SCIENCE DIRECT®

Journal of Sound and Vibration 267 (2003) 1107–1126

JOURNAL OF SOUND AND VIBRATION

www.elsevier.com/locate/jsvi

An analytical model to predict the response of fluid-filled shells to impact—a model for blunt head impacts

P.G. Young*

School of Engineering and Computer Science, University of Exeter, Harrison Building, North Park Road, Exeter, Devon, EX8 5LW, UK

Received 5 August 2002; accepted 29 October 2002

Abstract

An approximate analytical model to predict the response of a fluid-filled shell of arbitrary thickness impacting with a solid elastic sphere is proposed and the limits of applicability of the equations developed are discussed. The model is based on combining the Hertzian contact stiffness and the effective local membrane and bending stiffness to derive implicit expressions for global impact characteristics including the duration of impact, the peak force transmitted, peak global acceleration of shell and sphere, and the resultant pressures induced in the fluid. Closed-form explicit expressions are also derived to predict whether the pressure response in the fluid will be hydrostatic or will exhibit large dynamic transients of pressure (and shear strain). It should be noted that the impact of hollow/empty shells with solid spheres, as well as the impact of shells with an elastic half-space, can be straightforwardly treated as limiting cases. The model is of obvious relevance to head impact modelling and selected parametric studies of the response of fluid-filled shells with geometric and material properties about those typical for the human head are given.

1. Introduction

Research into the occurrence and prevention of head injury is driven by the considerable personal, societal and financial costs involved. Several sets of figures exist but, as a guide, for 1993 an estimated two million persons suffered brain injuries in the US alone and four-hundred thousand of these were hospitalized. Because of the scale of the problem, a broad range of research studies based on cadaveric, analytical or numerical techniques have been undertaken to characterize the response of the human head to impact and in particular to attempt to explain potential injury mechanisms.

*Tel.: +44-1392-263-684; fax: +44-1392-217-965.
E-mail address: philippe.g.young@exeter.ac.uk (P.G. Young).

0022-460X/03/$ - see front matter
doi:10.1016/S0022-460X(03)00200-1

Early analytical work includes that of Anzelius [1] who developed a model assuming the head to be a rigid spherical vessel filled with inviscid fluid. The impact was modelled as a delta function and equations were derived for determining the pressure within the liquid (inviscid, compressible) as a function of time. Guttinger [2] modelled the head in a similar manner, but rather than the shell travelling at a constant velocity and undergoing sudden arrest, his model describes the shell acquiring a time-dependent velocity from rest or uniform motion. Engin [3] proposed an analytical model, which included bending and membrane compliance of the shell, and studied the response for a fluid-filled sphere subjected to delta loading. This latter analysis was subsequently extended to loadings of finite duration by Kenner and Goldsmith [4].

More recently, the finite element method has become the numerical approach of choice, principally because of the ease with which irregular geometry and material non-linearities can be modelled. Many studies have been carried out and the reader is referred to three useful reviews of work on finite element models of head impacts [5–7]. Models have become increasingly sophisticated; Ruan et al. [8] simulated anatomical details including scalp, dura matter, falx cerebri and brain, giving the brain and scalp viscoelastic properties and the other tissues elastic properties; Bandak et al. [9] developed a geometrically very accurate patient-specific model of a human skull based on computed tomography imaging data with material properties assigned based on an empirical relationship between Hounsfield number and Young's modulus. Young and Morfey [10] returned to the problem of an elastic fluid-filled spherical shell and carried out an extensive parametric study on the response to an applied force–time history using the finite element approach. The authors were able to clearly identify regions of significant dynamic magnification of the intra-cranial pressure and found that the response could be conveniently collapsed on the impact duration over the period of the first mode of vibration of the system. An approximate closed-form expression for the period of this mode was then obtained by Young [11] and compared to results obtained using full three-dimensional elasticity equations.

To the author's knowledge, none of the previous work has approached the problem of developing closed-form expressions to predict the severity of impact (as determined for example by the head injury criterion, HIC) or other global characteristics such as the maximum force transmitted, the maximum acceleration and the impact duration. In fact, very little work has been done in modelling the contact mechanics of the problem, with both analytical and finite element models mostly based on assumed or experimentally determined force–time histories applied to the models. In the present paper an analytical model of the dynamic contact problem is developed in order to predict global impact characteristics. This model is then used to provide expressions for predicting the conditions under which a dynamic, rather than quasi-static, intra-cranial response might be expected. Although this model is based on a number of simplifying assumptions, important conclusions can be drawn regarding the response of the human head to impact. The author has presented some finite element [12,13] and some experimental [14] corroborations of this analytical model that demonstrate its predictive accuracy.

Although the primary motivation of the work is to study the response of the human head to impact, the analytical models developed can obviously be applied to a range of problems of interest in more traditional engineering areas involving the response of fluid-filled shell structures to impact.

2. Theory: impact of a fluid-filled shell of arbitrary thickness with a solid sphere

Consider the direct, rather than oblique, impact of two bodies: a fluid-filled spherical shell of mass m_{sh} travelling at a velocity v_{sh} and a solid sphere of mass m_{sol} travelling at a velocity v_{sol} as shown in Fig. 1. The outer radius of the shell is R_{sh}, the shell thickness is h and the shell material properties are assumed to be homogeneous and isotropic with a Young's modulus E_{sh}, a Poisson ratio v_{sh} and a density ρ_{sh}. The shell is filled with an inviscid fluid of density ρ_f and bulk modulus B and R_f is the outer radius of the fluid (inner radius of the shell). The radius of the solid sphere is R_{sol} and the material properties of the sphere are also assumed to be homogeneous and isotropic with Young's modulus E_{sol}, the Poisson ratio v_{sol} and a density ρ_{sol}.

2.1. Contact laws

The Hertzian contact stiffness between two solid spheres and the contact stiffness for a thin spherical shell with a uniform pressure applied on a small spherical cap will be considered independently of one another.

2.1.1. Hertzian contact stiffness k_H

Assuming a Hertzian contact model, the force deflection relationship between the two non-conforming bodies as given by Hertz [15] is

$$F = k_H \Delta x_H^{3/2}, \tag{1}$$

where F is the applied force, Δx_H is the mutual approach of distant points in the two solids, and the contact stiffness k_H is given by

$$k_H = \tfrac{4}{3} R^{*1/2} E^*, \tag{2}$$

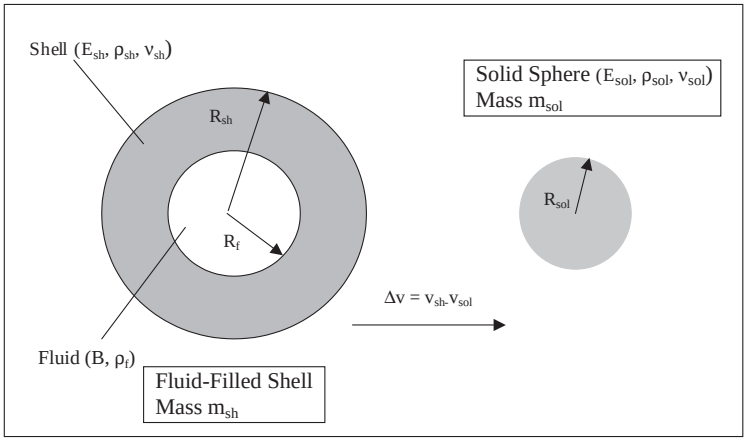

Fig. 1. Diagrammatic representation of impact model.

where

$$\frac{1}{R^*} = \frac{1}{R_{sol}} + \frac{1}{R_{sh}} \quad \text{and} \quad \frac{1}{E^*} = \frac{(1 - v_{sol}^2)}{E_{sol}} + \frac{(1 - v_{sh}^2)}{E_{sh}}.$$

The above contact stiffness is applicable for continuous smooth, frictionless and non-conforming contact surfaces providing:

(i) The ratio of the maximum contact–patch radius a to the relative radius of curvature R^* is small ($a/R^* \ll 1$).
(ii) The maximum contact radius a is small compared with the dimensions of each body. (This implies $a/h \ll 1$.)

2.1.2. Shell (membrane and bending) stiffness k_{sh}

For a thin empty spherical shell the maximum deflection Δx_{sh} from a force F applied as a uniform pressure on a small spherical cap of radius a ($a/R_{sh} \ll 1$) is given by

$$F = k_{sh} \Delta x_{sh}, \tag{3}$$

where the stiffness k_{sh} is given by [16]

$$k_{sh} = 2.3(E_{sh} h^2)/(R_{sh}(1 - v_{sh}^2)^{(1/2)}). \tag{4}$$

The applied pressure is resisted by both membrane and bending action in the shell. The above expression is an excellent approximation for:

(i) $a/h \ll 1$ providing $(4/27(h/R_{sh})^2(1 - v_{sh}^2))^{1/4} < 0.4$ which will hold true for $h/R_{sh} < 0.2$.
(ii) a/h not $\ll 1$ providing $a/(R_{sh}h)^{1/2}(12(1 - v_{sh}^2))^{1/4} < 0.4$. This latter condition can prove quite restrictive for very thin shells $h/R_{sh} \ll 1$ as one can quite clearly imagine impacts such that $a/R_{sh} \ll 1$ and $a/h \gg 1$.

There are several important points to note regarding the formulae given above:

(1) Eqs. (3) and (4) were shown in previous work by the author to be applicable to spherical shells filled with compressible or incompressible fluid; in other words, the bulk modulus of the fluid was shown to have no effect on the stiffness of the shell.
(2) The region over which both membrane and bending deformations predominantly occur is very localized and limited at most to a half-angle θ about the centre of the applied pressure given by $\theta = \arcsin(1.65(h/R_{sh}))$. For $h/R_{sh} < 0.2$ this implies that the stiffness is significantly influenced by at most a 20° half-angle about the centre of pressure. This is significant as, from a stiffness perspective, one need only consider the structure in a small window about the impact site (i.e., one can conveniently, within limits, disregard structural characteristics, such as material properties and the geometry, outside this window).
(3) The linear stiffness given by equation k_{sh} is not a function of the circular planform area (of radius a) over which the pressure is applied. This is important, as this area is not constant for non-conforming contacts. By implication it is also not a function of the pressure distribution on the spherical cap, which is also, in the case of contact problems, non-uniform.

2.2. Analytical model: implicit equation for F_{max}

The Hertzian contact stiffness k_H and the shell contact stiffness k_{sh} will be considered decoupled and the system will be solved assuming the two stiffnesses can be considered in series. This decoupling is based on assuming that the contact–patch area is determined solely by the Hertzian contact mechanics and that the local deformations due to compliance of the shell do not appreciably increase this area. Since the shell stiffness k_{sh} is not a function of the contact area, introducing this assumption will not influence the compliance of the shell (membrane and bending deformations) however it would tend to underestimate the effective Hertzian contact stiffness.

Assuming a conservative system and applying the principle of conservation of energy gives

$$\tfrac{1}{2}m_{sh}v_{sh}^2 + \tfrac{1}{2}m_{sol}v_{sol}^2 = \tfrac{1}{2}k_{sh}\Delta x_{sh}^2 + \tfrac{2}{5}k_H\Delta x_H^{5/2} + \tfrac{1}{2}(m_{sh}+m_{sol})v_{sh-sol}^2, \tag{5}$$

where Δx_{sh} is the deformation due to membrane and bending action in the shell, v_{sh-sol} is the velocity of the shell–sphere system at the point of maximum compression and Δx_H is the deformation due to the Hertzian contact deformations in both the shell and the solid sphere combined.

Applying the principle of conservation of momentum

$$m_{sh}v_{sh} + m_{sol}v_{sol} = (m_{sh}+m_{sol})v_{sh-sol}. \tag{6}$$

Solving Eq. (6) for v_{sh-sol}:

$$v_{sh-sol} = \frac{(m_{sh}v_{sh} + m_{sol}v_{sol})}{(m_{sh}+m_{sol})}. \tag{7}$$

The maximum deformations Δx_{sh} and Δx_H can straightforwardly be expressed in terms of the maximum force transmitted F_{max}:

$$\Delta x_{sh} = F_{max}/k_{sh} \quad \text{and} \quad \Delta x_H = (F_{max}/k_H)^{2/3}. \tag{8}$$

Substituting Eqs. (7) and (8) into Eq. (5) and rearranging

$$m^*\Delta v^2 = \frac{F_{max}^2}{k_{sh}} + \frac{4}{5}\frac{F_{max}^{5/3}}{k_H^{2/3}}, \tag{9}$$

where $\Delta v = v_{sh} - v_{sol}$ and $1/m^* = 1/m_{sh} + 1/m_{sol}$.

Expression (9) is an implicit (and approximate) expression for the maximum force transmitted F_{max} which includes both the effects of Hertzian contact deformations in shell and sphere and local membrane and bending action in the shell. Eq. (9) can be solved numerically for F_{max} and the maximum deformations and the acceleration of the fluid-filled shell can then be expressed straightforwardly as

$$\Delta x = \Delta x_{sh} + \Delta x_H = \frac{F_{max}}{k_{sh}} + \left(\frac{F_{max}}{k_H}\right)^{2/3}, \tag{10}$$

$$a_{max} = \frac{F_{max}}{m_{sh}}. \tag{11}$$

The time of impact T_p can then be obtained by numerical integration of the force–deflection curve. Alternatively, if simple harmonic motion is assumed with an effective linear stiffness k_{effec}

given by

$$k_{effec} = \frac{F_{max}}{\Delta x} = 1/\left(\frac{1}{k_{\mathrm{sh}}} + \frac{1}{k_H^{2/3} F_{max}^{1/3}}\right), \tag{12}$$

the time of impact T_p can be approximated by

$$T_p = \pi\sqrt{\frac{m^*}{k_{effec}}}. \tag{13}$$

The *HIC*, a commonly used measure of the severity of an impact to the head, is defined by the expression

$$HIC = \max(t_1, t_2)\left\langle \frac{1}{(t_2 - t_1)^{3/2}}\left[\int_{t_1}^{t_2} a(t)\,\mathrm{d}t\right]^{5/2}\right\rangle, \tag{14}$$

where the notation $\max(t_1 : t_2)$ signifies that the time interval t_1 to t_2 is chosen to maximize the expression in brackets. Assuming the acceleration of the head $a(t)$ is given by

$$a(t) = \frac{F_{max}}{m_{sh}} \sin\left(\pi \frac{t}{T_p}\right) \tag{15}$$

for $0 < t < T_p$, the time interval which maximizes expression (14) can straightforwardly be obtained by substituting Eq. (15) into Eq. (14) and solving simultaneously

$$\begin{aligned} \frac{\partial(HIC)}{\partial t_1} &= 0, \\ \frac{\partial(HIC)}{\partial t_2} &= 0 \end{aligned} \tag{16}$$

to give $t_1/T_p = 0.1648852$ and $t_2/T_p = 0.8351148$. Substituting back into expression (14) gives

$$\begin{aligned} HIC &= \frac{7.25311}{\pi^{5/2}} \frac{F_{max}}{M_{sh}} T_p \\ &= \frac{7.25311}{\pi^{3/2}} F_{max} \sqrt{\left(\frac{1}{k_{\mathrm{sh}}} + \frac{1}{k_H^{2/3} F_{max}^{1/3}}\right)\left(\frac{m_{sol}}{m_{sh}(m_{sol} + m_{sh})}\right)}. \end{aligned} \tag{17}$$

2.3. Limiting cases

Consider two limiting cases: Case I, Hertzian impact neglecting shell bending/membrane deformations; and Case II, shell impact with a rigid ball neglecting local Hertzian deformations.

Limiting Case I, $k_{sh} \ll k_H$: Neglecting the contribution of the Hertzian contact spring or, in other words, assuming $k_H \to \infty$ expressions (9)–(11) and (13) reduce to

$$m^* \Delta v^2 = \frac{F_{max}^2}{k_{sh}}, \tag{18}$$

$$F_{max} = \sqrt{\frac{2.3E_{sh}h^2m^*\Delta v^2}{R_{sh}\sqrt{(1-v_{sh}^2)}}}, \tag{19}$$

$$\Delta x_{sh} = \frac{F_{max}}{k_{sh}} = \Delta v\sqrt{\frac{m^*R_{sh}\sqrt{(1-v_{sh}^2)}}{2.3E_{sh}h^2}}, \tag{20}$$

$$T_p = \pi\sqrt{\frac{m^*}{k_{sh}}} = \pi\sqrt{\frac{m^*R_{sh}\sqrt{(1-v_{sh}^2)}}{2.3E_{sh}h^2}}, \tag{21}$$

$$a_{max} = \frac{F_{max}}{m_{sh}} = \sqrt{\frac{2.3E_{sh}h^2m^*\Delta v^2}{m_{sh}^2R_{sh}\sqrt{(1-v_{sh}^2)}}}. \tag{22}$$

Limiting Case II, $k_{sh} \gg k_H$: Neglecting the contribution from local membrane and bending action in the shell, or in other words assuming $k_{sh} \to \infty$, the problem reduces to the classical Hertzian quasi-static impact theory

$$m^*\Delta v^2 = \frac{4}{5}\frac{F_{max}^{5/3}}{k_H^{2/3}}, \tag{23}$$

$$F_{max} = \left(\frac{5}{4}k_H^{2/3}m^*\Delta v^2\right)^{3/5} = \frac{4}{3}\left(\frac{15}{16}\right)^{3/5}R^{*1/5}E^{*2/5}m^{*3/5}(\Delta v)^{6/5}, \tag{24}$$

$$a_{max} = \frac{4}{3}\left(\frac{15}{16}\right)^{3/5}R^{*1/5}E^{*2/5}\frac{m^{*3/5}}{m_{sh}}(\Delta v)^{6/5}, \tag{25}$$

$$\Delta x_H = \left(\frac{F_{\max}}{k_H}\right)^{2/3} = \frac{15}{16}\frac{m^*\Delta v^2}{R^{*1/2}E^*}. \tag{26}$$

The time of impact obtained by numerical integration of the force–deflection curve [17] is given by

$$T_p = 2.87\left(\frac{m^{*2}}{R^*E^{*2}\Delta v}\right)^{1/5}. \tag{27}$$

Alternatively, if simple harmonic motion is assumed with a stiffness k_{linear} given by

$$k_{linear} = \frac{F_{max}}{\Delta x_H} = \frac{4}{3}\left(\frac{15}{16}\right)^{1/5}R^{*2/5}E^{*4/5}m^{*1/5}\Delta v^{2/5}, \tag{28}$$

the impact duration will be approximately given by

$$T_p = \pi\sqrt{\frac{m^*}{k_{linear}}} = 2.74\left(\frac{m^{*2}}{R^*E^{*2}\Delta v}\right)^{1/5}, \tag{29}$$

which is close to expression (27) obtained by numerical integration of the force–deflection curve. This implies that for the more general case, where both the effect of shell action and Hertzian contact stiffness are included, using an effective linear stiffness as given by Eq. (12) to obtain an approximate time of impact, rather than the more accurate integration of the force–deflection curve, will, at most, underestimate the time of impact by 5% ($(2.74-2.87)/2.87\times100 = -4.5\%$).

2.4. Simplified analytical model: explicit expression for F_{max}

Although the implicit expression given by Eq. (9) can straightforwardly be solved for F_{max} from which the other impact characteristics can be obtained, in order to draw some interesting conclusions it will prove useful to obtain approximate explicit expressions. Explicit expressions can be obtained by introducing a further simplification, namely that the Hertzian contact stiffness is given by Eq. (28). The approximate linear stiffness of the system k'_{effec} combining the linearized Hertzian stiffness (Eq. (28)) and the shell-membrane stiffness (Eq. (4)) will be given by

$$\begin{aligned} k'_{effec} &= \frac{k_{linear}k_{sh}}{(k_{linear}+k_{sh})} \\ &= \frac{R^{*2/5}E^{*4/5}m^{*1/5}\Delta v^{2/5}E_{sh}h^2}{\left[\dfrac{1}{2.3}R^{*2/5}E^{*4/5}m^{*1/5}\Delta v^{2/5}R_{sh}\sqrt{(1-v_{sh}^2)}+\dfrac{3}{4}\left(\dfrac{16}{15}\right)^{1/5}E_{sh}h^2\right]}. \end{aligned} \tag{30}$$

It should be stressed that using the above expression for the stiffness of the system is not equivalent to solving the implicit Eq. (9) for F_{max} and then obtaining the effective linear stiffness k_{effec} from Eq. (12) (except, of course, for the special case $k_{sh}\to\infty$). Since the Hertzian contact stiffness is a stiffening non-linear spring ($F = k_H\Delta x_H^{3/2}$) and the above assumption approximates the effective linear stiffness of the Hertzian spring by assuming the impact is wholly absorbed by the Hertzian spring, the overall stiffness will be overestimated. Using Eq. (30) will therefore provide an upper bound on both the peak force transmitted and the acceleration of the system and a lower bound on the impact duration. Explicit equations can now be obtained and are given by

$$m^*\Delta v^2 = \frac{F_{max}^2}{k'_{effec}}, \tag{31}$$

$$F_{max} = \frac{R^{*1/5}E^{*2/5}m^{*3/5}\Delta v^{6/5}E_{sh}^{1/2}h}{\left[\dfrac{1}{\sqrt{2.3}}R^{*1/5}E^{*2/5}m^{*1/10}\Delta v^{1/5}R_{sh}^{1/2}(1-v_{sh}^2)^{1/4}+\dfrac{\sqrt{3}}{2}\left(\dfrac{16}{15}\right)^{1/10}E_{sh}^{1/2}h\right]}, \tag{32}$$

$$a_{max} = \frac{F_{max}}{m_{sh}}, \tag{33}$$

$$\Delta x = \Delta v\sqrt{\frac{3}{4}\left(\frac{16}{15}\right)^{1/5}\frac{m^{*4/5}}{R^{*2/5}E^{*4/5}\Delta v^{2/5}}+\frac{m^*R_{sh}\sqrt{(1-v_{sh}^2)}}{2.3E_{sh}h^2}}, \tag{34}$$

$$T_p = \pi\sqrt{\frac{3}{4}\left(\frac{16}{15}\right)^{1/5}\frac{m^{*4/5}}{R^{*2/5}E^{*4/5}\Delta v^{2/5}} + \frac{m^* R_{sh}\sqrt{(1-v_{sh}^2)}}{2.3E_{sh}h^2}}. \tag{35}$$

2.5. Pressure response in the fluid: predicting the onset of high-pressure transients

In previous work by Young and Morfey [10] it was shown that the onset of dynamic effects for fluid-filled spherical shells, and in particular the onset of large positive and negative pressure transients at the pole and anti-pole, could be conveniently predicted using the ratio of the period of oscillation of the first $n = 2$ spheroidal mode of vibration of the fully free shell T_Ω and the duration of impact T_P. It was later shown that the first $n = 2$ spheroidal mode of vibration was equi-voluminal and, for a very wide range of thicknesses, dominated by membrane action [11]. An approximate closed-form expression that accurately predicts the period of oscillation T_Ω was derived based on the exact solution for a membrane filled with incompressible fluid for the spherical shell case

$$T_\Omega = \sqrt{\frac{3\pi(5+v_{sh})m_{sh}}{8hE_{sh}}}. \tag{36}$$

For $h/R_f < 0.4$ and for $E/B \times h/R_f < 1$, the maximum error in using the above approximate equation was shown to be less than 10% when compared with solving the problem using full three-dimensional elasticity equations.

It was shown in Ref. [10] that for a ratio of impact duration T_p to period of oscillation T_Ω greater than approximately 4 ($T_p/T_\Omega > 4$) the pressure response in the fluid was essentially hydrostatic, with a linear pressure gradient varying from a maximum positive peak pressure P_{quasi} under the site of impact (pole) to a minimum negative peak pressure $-P_{quasi}$ at the anti-pole. Here P_{quasi} is straightforwardly given by

$$P_{quasi} = R_f \rho_f F_{max}/m_{sh}. \tag{37}$$

For shorter impact durations ($T_p/T_\Omega < 4$) dynamic transient pressures were observed at both the pole and anti-pole, with increasingly high peak pressures as this ratio dropped significantly below 2 (up to eight times those predicted by the hydrostatic equation above). For more information on these pressure transients the reader is referred to the work by Young and Morfey [10].

In the case of a Hanning[1] force–time history applied radially over a small spherical cap, the dynamic magnification is approximately given by

$$\frac{P_{max}}{P_{quasi}} = -32\mathrm{e}^{-2(T_p/T_\Omega)}. \tag{38}$$

Eq. (38) gives the ratio of the maximum negative pressure P_{max} in the fluid directly under the site of impact (at the pole) over the quasi-static pressure P_{quasi}; it has been obtained based on

[1] A Hanning force–time history [$F(t) = F_{max}(1/2 - 1/2(\cos(\pi t/T_p))$] is a reasonable approximation of the actual force–time history for an impact which will lie between a half-sine [$F(t) = F_{max}\sin(\pi t/T_p)$] and a half-sine to the 3/2 [$F(t) = F_{max}\sin(\pi t/T_p)^{3/2}$] depending on the relative contributions of the Hertzian and shell/membrane stiffnesses.

numerical results given in Ref. [10] for T_p/T_Ω values between 0.5 and 2 ($R^2 > 0.97$). By using the analytical model presented above, the impact duration T_p can be predicted and the likelihood of the pressure response in the fluid exhibiting large dynamic pressure transients can be assessed. This can be done on a case by case basis by solving the implicit equation for F_{max} (Eq. (9)), and then obtaining the ratio T_p/T_Ω.

However, in order to be able to draw a priori some broad conclusions regarding the nature of the pressure response in the fluid, an approximate explicit expression can be obtained based on the simplified explicit expressions derived above in Section 2.4.

2.5.1. Approximate explicit expression for T_p/T_Ω

Using the approximate expression for the time of impact T_p given by Eq. (35) and the approximate expression for T_Ω given by Eq. (36), an approximate explicit expression for T_p/T_Ω can be obtained.

As was previously discussed, T_p is underestimated by expression (35) and the resultant expression for T_p/T_Ω will therefore probably be a lower bound. Since the approximate expression derived for T_Ω is applicable to fluid-filled spherical shells only, the mass of the shell m_{sh} can be expressed as

$$m_{sh} = \frac{4}{3}\pi R_{sh}^3 \rho_{sh}\left[\frac{\rho_f}{\rho_{sh}} + \left(3\frac{h}{R_{sh}} - 3\left(\frac{h}{R_{sh}}\right)^2 + \left(\frac{h}{R_{sh}}\right)^3\right)\left(1 - \frac{\rho_f}{\rho_{sh}}\right)\right]. \tag{39}$$

On introducing the above expression for m_{sh} into Eqs. (35) and (36) and simplifying, the following expression for T_p/T_Ω is obtained

$$\frac{T_P}{T_\Omega} = \sqrt{\left(\frac{\left(\frac{128}{5}\right)^{1/5}\frac{\pi^{4/5}}{(5+\nu_{sh})}\left(\frac{c}{\Delta v}\right)^{2/5}\left(\frac{h}{R_{sh}}\right)\left(\frac{m_{sol}}{m_{sol}+m_{sh}}\right)^{4/5}\left(1+\frac{R_{sh}}{R_{sol}}\right)^{2/5}\left((1-\nu_{sh}^2)+(1-\nu_{sol}^2)\frac{E_{sh}}{E_{sol}}\right)^{4/5}}{\left[\frac{\rho_f}{\rho_{sh}}+\left(3\frac{h}{R_{sh}}-3\left(\frac{h}{R_{sh}}\right)^2+\left(\frac{h}{R_{sh}}\right)^3\right)\left(1-\frac{\rho_f}{\rho_{sh}}\right)\right]^{1/5}\left(1+\frac{m_{sh}}{m_{sol}}\right)^{4/5}} + \left(\frac{8\pi}{6.9}\left(\frac{R_{sh}}{h}\right)\frac{(1-\nu_{sh}^2)^{1/2}}{(5+\nu_{sh})\left(1+\frac{m_{sh}}{m_{sol}}\right)}\right)\right)}. \tag{40}$$

Here c is the wave speed in the shell given by $c = (E_{sh}/\rho_{sh})^{(1/2)}$. Eq. (40) is an expression for T_p/T_Ω as a function of the non-dimensional parameters m_{sol}/m_{sh}, R_{sol}/R_{sh}, E_{sol}/E_{sh}, h/R_{sh}, $c/\Delta v$, ν_{sh}, ν_{sol} and ρ_f/ρ_{sh}. The first term under the square root represents the contribution from the Hertzian contact deformation and the second term represents the contribution from the shell-membrane and bending deformations. It is interesting to note that the ratio T_p/T_Ω increases as a function of $(h/R_{sh})^{(1/2)}$ for the Hertzian contact component, but increases as a function of $1/(h/R_{sh})^{(1/2)}$ for the shell-membrane and bending component. One should also note that T_p/T_Ω is not a function of the bulk modulus of the fluid as neither the impact duration nor the period of oscillation are functions of the bulk modulus.

3. Results and discussion

A series of parametric studies for values about those typical for the human head has been carried out by the author and results obtained using the analytical equations have been compared to numerical results obtained using both finite element and experimental models and some preliminary results have been presented in Refs. [12–14]. However, it is instructive at this stage if the analytical equations derived above are used to explore the response for a range of parameter values and for a number of special cases. It should be stressed that in some cases portions of the curves plotted will lie outside the range of applicability of the proposed theory. It is also important to recall that the derived equations are only valid for small deformations and assume a linear elastic material response.

3.1. Peak transmitted force: select parametric studies and comparison with shell and Hertz theories

An alternative non-dimensional implicit expression equivalent to Eq. (9) can be derived which will be useful for exploring the behaviour of the system to changes in various parameters. In general, the mass of the shell can be expressed as

$$m_{sh} = R^3 \rho_{sh}\, densfunc\left(\frac{\rho_f}{\rho_{sh}}, \frac{h}{R}\cdots\right), \tag{41}$$

where R is a characteristic length of the shell and *densfunc* is a non-dimensional function of the geometry and density of the shell. For the particular case of a fluid-filled spherical shell m_{sh} is given by Eq. (39), where $R = R_{sh}$ and

$$densfunc = \frac{4}{3}\pi\left[\frac{\rho_f}{\rho_{sh}} + \left(3\frac{h}{R_{sh}} - 3\left(\frac{h}{R_{sh}}\right)^2 + \left(\frac{h}{R_{sh}}\right)^3\right)\left(1 - \frac{\rho_f}{\rho_{sh}}\right)\right].$$

Substituting expressions for k_{sh} and k_H Eqs (2) and (4) into Eq. (9) as well as expression (41) for m_{sh} and after some rearranging we have

$$\begin{aligned}&\left(\frac{F_{max}}{E_{sh}R^2}\right)^2\left(\frac{R}{h}\right)^2\left(\frac{c}{\Delta v}\right)^2\left(1 + \frac{m_{sh}}{m_{sol}}\right)\frac{\sqrt{1 - v_{sh}^2}}{2.3}\\ &\quad + \frac{3}{5}\left(\frac{F_{max}}{E_{sh}R^2}\right)^{5/3}\left(\frac{c}{\Delta v}\right)^2\left(1 + \frac{m_{sh}}{m_{sol}}\right)\left(1 + \frac{R_{sh}}{R_{sol}}\right)^{1/3}\\ &\quad \times\left((1 - v_{sh}^2) + (1 - v_{sol}^2)\frac{E_{sh}}{E_{sol}}\right)^{2/3} - \frac{m_{\mathrm{sh}}}{R^3\rho_{sh}} = 0.\end{aligned} \tag{42}$$

The first term in the equation is due to local membrane and bending deformations and the second term is from the localized Hertzian deformation.

The non-dimensional maximum force transmitted parameter $F_{max}/E_{sh}R_{sh}^2$ was computed using this equation and also by alternately neglecting the Hertzian stiffness component and the membrane/bending stiffness component; the three different solutions obtained in this manner are referred to in the graphs as the combined, shell and Hertz solutions, respectively. Impacts were against a rigid ($E_{sh}/E_{sol} = 0$) half-space (infinite mass $m_{sh}/m_{sol} = 0$ and flat contact surface

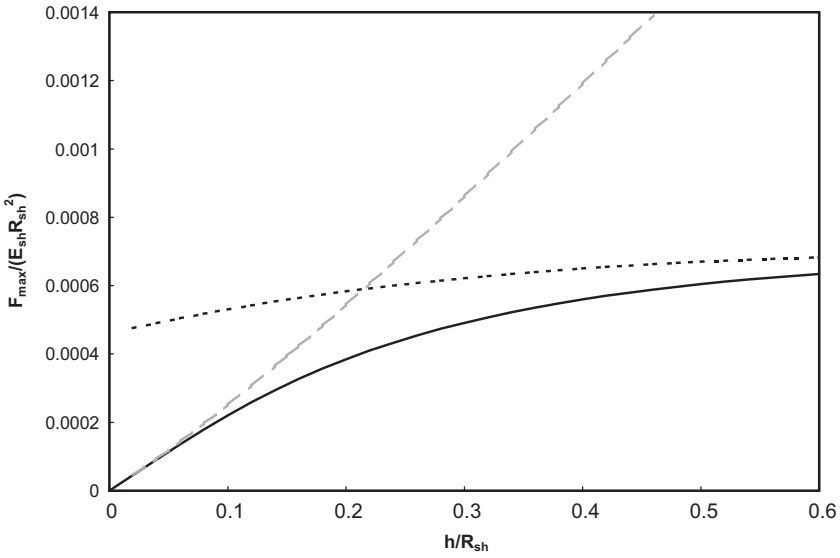

Fig. 2. Non-dimensional maximum force transmitted $F_{max}/(E_{sh}R_{sh}^2)$ as computed using shell only theory, Hertz only theory and combined theory for a range of shell thicknesses. (——) Combined; (– – –) shell; (- - - -) Hertz.

$R_{sh}/R_{sol} = 0$). The Poisson ratio of the shell was assumed to be 0.25 and the density ratio was assumed to be $\rho_f/\rho_{sh} = 1/2$ (approximate ratio for the density of brain to skull bone).

In Fig. 2 $F_{max}/E_{sh}R_{sh}^2$ is plotted for a range of thickness ratios h/R_{sh} ranging from 0 to 0.6 for a wave speed ratio $c/\Delta v$ equal to 1000 (approximately equivalent to a 2.5 m/s impact for skull bone). As would be expected, for small thickness ratios the peak force transmitted decreases and the shell theory solution tends towards the combined solution as the flexibility of the shell dominates. On the other hand for thicker shells, the Hertzian flexibility is dominant and the peak force transmitted predicted by the Hertzian theory tends towards the combined solution. What is surprising, however, is the range of thickness ratios for which neither Hertz nor shell solutions provide accurate results. This is shown more clearly in Fig. 3 where the percentage difference between the shell and combined solutions and Hertz and combined solution are plotted. If both stiffness components are not considered, the error is greater than 15% for shell thickness ratios between $\frac{1}{10}$ and $\frac{2}{5}$.

In Fig. 4 $F_{max}/E_{sh}R_{sh}^2$ is plotted for a range of wave speed ratios ranging from close to zero to $\frac{1}{1000}$ for a thickness ratio $h/R_{sh} = 1/5$. Because of the non-linear spring stiffening behaviour of the Hertzian component of stiffness for low impact velocities the flexibility is dominated by the Hertzian component, whereas for higher impact velocities the shell flexibility component becomes more significant. This is shown clearly in Fig. 5 where the percentage error is again plotted for both the Hertz and shell theories when compared with the combined theory.

3.2. Special case: constant energy impacts ($1/2\, m^* \Delta v^2$=constant)

For impacts on a fluid-filled shell of constant impact kinetic energy $1/2\, m^* \Delta v^2$ it is obvious from Eqs (9)–(11) that the peak force F_{max}, peak acceleration a_{max} and the deformations Δx_H and Δx_{sh}

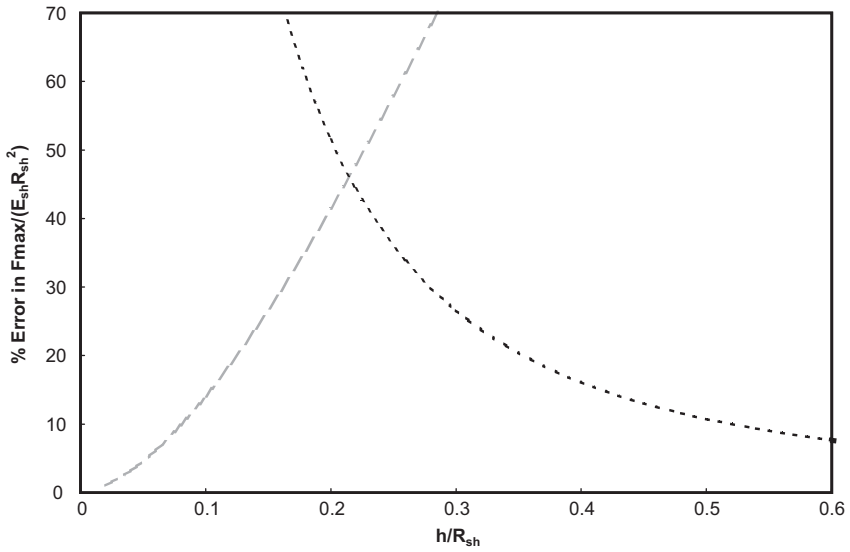

Fig. 3. Percentage error in non-dimensional maximum force transmitted $F_{max}/(E_{sh}R_{sh}^2)$ from using shell only theory and Hertz only theory versus combined theory for a range of shell thicknesses. (– – –) Shell; (- - - -) Hertz.

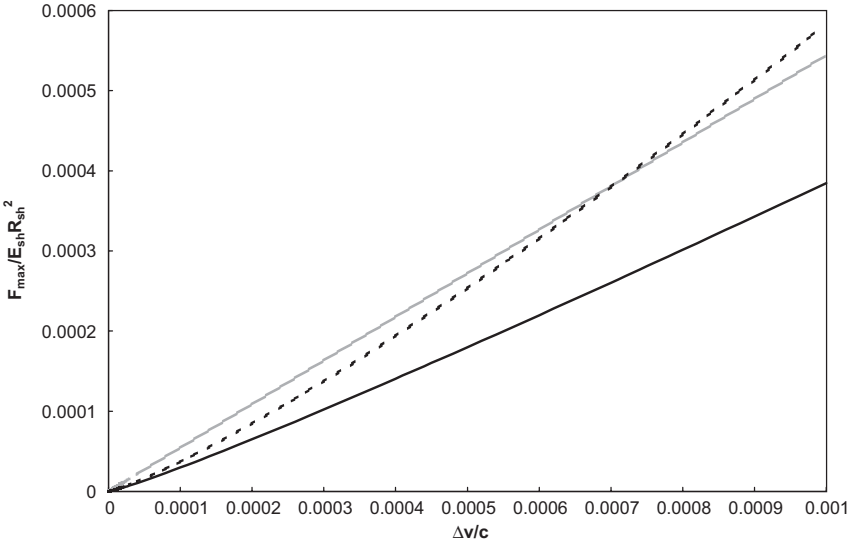

Fig. 4. Non-dimensional maximum force transmitted $F_{max}/(E_{sh}R_{sh}^2)$ as computed using shell only theory, Hertz only theory and combined theory for a range of impact velocities. (——) Combined; (– – –) shell; (- - - -) Hertz.

predicted will not be a function of m^* (i.e., not a function of m_{sol}/m_{sh}). However, the time of impact T_p, as given by Eq. (13), will clearly vary as a function of $\sqrt{m^*}$. Defining T_∞ as the impact duration, HIC_∞ as the HIC value and F_∞ as the maximum force transmitted for an impact of given energy with a ball of infinite mass (i.e., $m_{sol}/m_{sh} \to \infty$, or equivalently $m^* \to m_{sh}$), then the

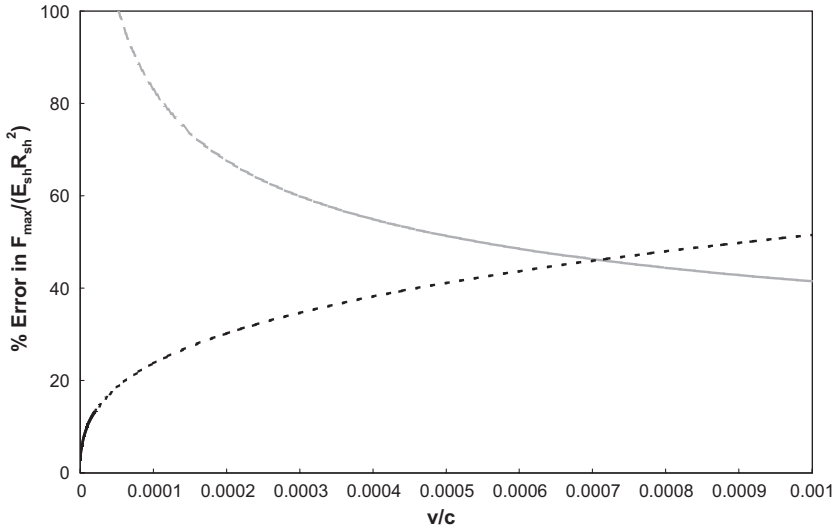

Fig. 5. Percentage error in the non-dimensional maximum force transmitted $F_{max}/(E_{sh}R_{sh}^2)$ from using shell only theory and Hertz only theory versus combined theory for a range of impact velocities. (– – –) Shell; (- - - -) Hertz.

ratios T_p/T_∞ and HIC/HIC_∞ are given by the same expression

$$\frac{T_p}{T_\infty} = \frac{HIC}{HIC_\infty} = \sqrt{\left(1/\left(1+\frac{m_{sh}}{m_{sol}}\right)\right)} \tag{43}$$

and F_{max}/F_∞ is given by

$$\frac{F_{max}}{F_\infty} = 1, \tag{44}$$

which are plotted in Fig. 6. As the mass of the impactor decreases both the durations of impact and the *HIC* values drop but the maximum force transmitted remains constant.

Defining Δv_∞ as the impact velocity with a projectile of infinite mass of equivalent energy to the impact considered, or in other words

$$\tfrac{1}{2} m_{sh} \Delta v_\infty^2 = \tfrac{1}{2} m^* \Delta v^2 \tag{45}$$

then,

$$\Delta v/\Delta v_\infty = (m_{sh}/m^*)^{1/2} \tag{46}$$

substituting Eq. (44) into the approximate expression for T_p/T_Ω given by Eq. (40) and rearranging a useful expression for T_p/T_Ω for impacts of constant energy is obtained

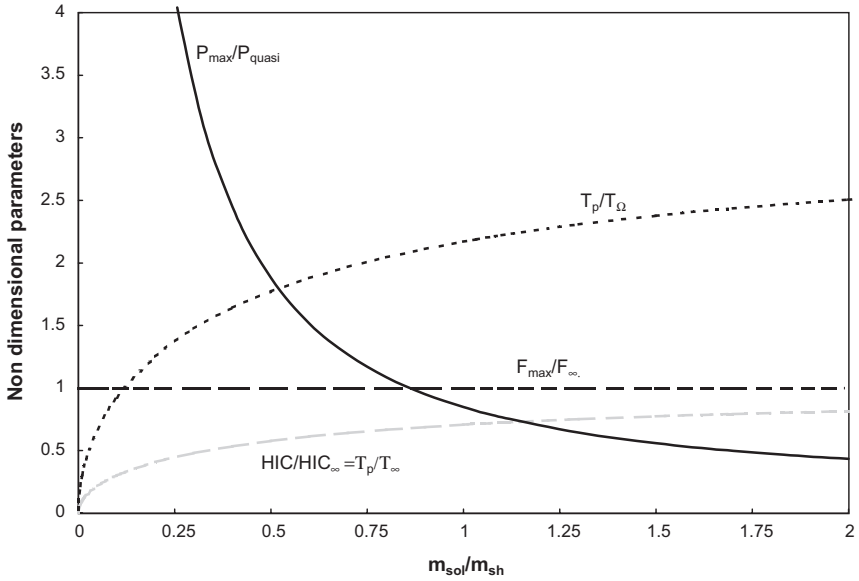

Fig. 6. Non-dimensional parameters for maximum pressure, maximum force, HIC and time of impact for constant energy impacts for a range of non-dimensional mass of projectile to mass of shell ratios. (——) P_{max}/P_{quasi}; (- - - -) T_p/T_Ω; (— — -) F_{max}/F_∞; (– – –) $HIC/HIC_\infty = T_P/T_\infty$.

$$\frac{T_p}{T_\Omega} = \sqrt{\frac{1}{1+\dfrac{m_{sh}}{m_{sol}}}} \sqrt{\frac{\left(\frac{128}{5}\right)^{1/5}\frac{\pi^{4/5}}{(5+\nu_{sh})}\left(\frac{c}{\Delta v_\infty}\right)^{2/5}\left(\frac{h}{R_{sh}}\right)\left(\frac{R_{sol}+R_{sh}}{R_{sol}}\right)^{2/5}\left((1-\nu_{sh}^2)+(1-\nu_{sol}^2)\frac{E_{sh}}{E_{sol}}\right)^{4/5}}{\left[\frac{\rho_f}{\rho_{sh}}+\left(3\frac{h}{R_{sh}}-3\left(\frac{h}{R_{sh}}\right)^2+\left(\frac{h}{R_{sh}}\right)^3\right)\left(1-\frac{\rho_f}{\rho_{sh}}\right)\right]^{1/5}} + \left(\frac{8\pi}{6.9}\left(\frac{R_{sh}}{h}\right)\frac{(1-\nu_{sh}^2)^{1/2}}{(5+\nu_{sh})}\right)}.$$

(47)

For the impact of a rigid flat projectile ($E_{sh}/E_{sol} \to 0$, $R_{sh}/R_{sol} \to 0$) on a fluid-filled shell of thickness ratio $h/R_{sh} = 0.1$, of density ratio $\rho_f/\rho_{sh} = 1/2$, the Poisson ratio $\nu_{sh} = 0.25$ and $c/\Delta v_\infty = 1000$, the ratio P_{max}/P_{quasi} (maximum negative pressure at the pole over quasi-static positive pressure prediction—Eq. (38)) will be given by

$$\frac{P_{max}}{P_{quasi}} = -32\mathrm{e}^{-6.14\sqrt{(1/(1+m_{sh}/m_{sol}))}},$$

which is plotted along with T_p/T_Ω, against m_{sh}/m_{sol} in Fig. 6. The graph clearly shows that the HIC value decreases with decreasing projectile mass, whereas the observed peak pressures increase rapidly; there is therefore an obvious and dramatic disagreement between use of peak pressure (whether positive or negative) as an injury criterion and the HIC for impacts with low mass projectiles. It must be stressed however that as the peak pressures increase dramatically, the

duration of these peak pressures decreases which might significantly affect their potential to cause damage [18].

3.3. Onset of large pressure transients in the fluid: select parametric studies

3.3.1. Impact with a rigid infinite mass

Consider the impact of a fluid-filled shell with a rigid infinite mass ($E_{sol}/E_{sh} \to \infty$, $m_{sol}/m_{sh} \to \infty$) and assume the Poisson ratio of the shell v_{sh} to be 0.25, the density of the fluid to density of the shell to be $\rho_f/\rho_{sh} = 1/2$ and the wave speed to impact velocity ratio to be $c/\Delta v = 1000$. In Fig. 7, the non-dimensional ratio T_p/T_Ω (as computed using Eq. (40)) is plotted against the thickness ratio h/R_{sh} for a number of radius of curvature ratios: $R_{sh}/R_{sol} = 0$ (a flat impact surface), $R_{sh}/R_{sol} = 10$ (a curved convex impact surface) and $R_{sh}/R_{sol} = -0.9$ (a concave impact surface almost conforming to the shell radius of curvature). For convex surfaces the non-dimensional ratio is higher as the Hertzian contact stiffness is lower and tends to a minimum as the impact surface becomes progressively concave (tends to a conforming impact). However, it can be seen that the ratio T_p/T_Ω does not drop below a value of 2 for the range of thickness ratios considered here ($0 < h/R_{sh} < 0.3$). The implication is that for impacts with an infinite mass object (e.g., the ground), significant dynamic pressure transients are unlikely to occur.

3.3.2. Influence of m_{sh}/m_{sol}: predicting the onset of dynamic effects

Eq. (40) can be solved for $T_p/T_\Omega = 2$ for a range of parameter values in order to establish an approximate boundary between high-pressure transients developing in the fluid and a quasi-static

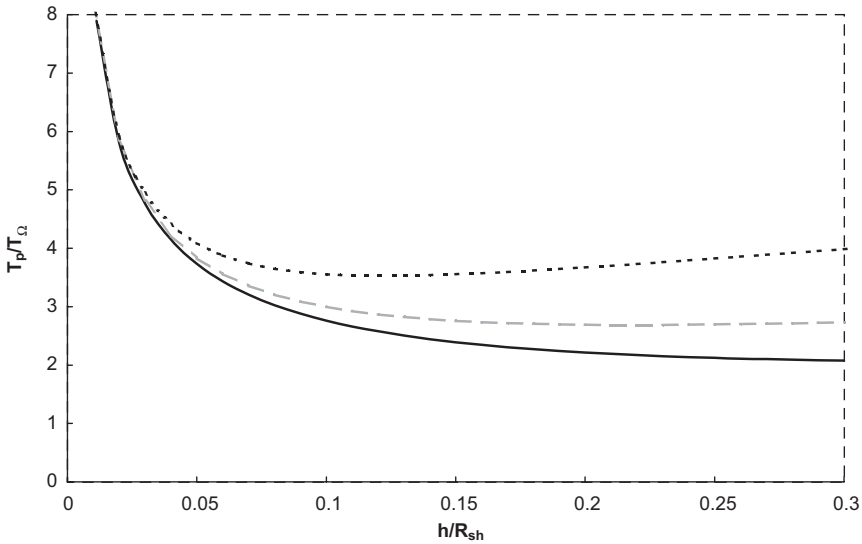

Fig. 7. Non-dimensional impact duration T_p/T_Ω against thickness ratio h/R_{sh} for a range of relative radius of curvature ratios R_{sh}/R_{sol}. (——) $R_{sh}/R_{sol} = 0.9$; (– – –) $R_{sh}/R_{sol} = 0$; (- - - -) $R_{sh}/R_{sol} = 10$.

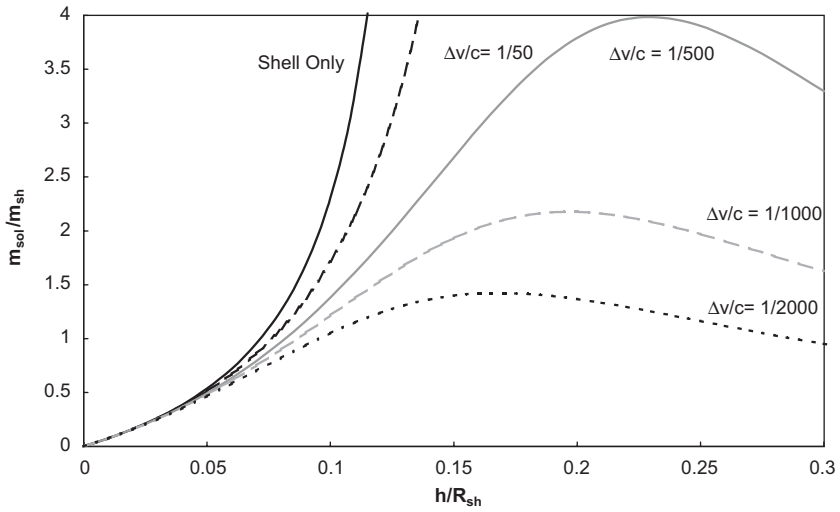

Fig. 8. Non-dimensional mass ratios m_{sh}/m_{sol} delimiting approximate boundaries between quasi-static and dynamic intra-cranial response against thickness ratios h/R_{sh} for a range of non-dimensional impact velocities $\Delta v/c$. (——) Shell; (– – -) $\Delta v/c = 1/50$; (—) $\Delta v/c = 1/500$; (– – –) $\Delta v/c = 1/1000$; (- - - -) $\Delta v/c = 1/2000$.

regime. Let us assume for all cases that the impactor has zero, or negligible, curvature at the impact site (in other words a flat impact surface, $R_{sh}/R_{sol} = 0$).

In Fig. 8 the mass ratio m_{sol}/m_{sh} for which T_p/T_Ω is equal to 2 is plotted against h/R_{sh} for a number of impact velocity to wave speed ratios $\Delta v/c$ ranging from $\frac{1}{50}$ (approximately equivalent to a 100 m/s impact velocity for a steel shell and 50 m/s for skull bone- and clearly outside the range of applicability of the equations given) to $\frac{1}{2000}$ (approximately 2.5 m/s impact for steel shell and 1.25 m/s for skull bone). For this case $\rho_f/\rho_{sh} = 1/2$, $E_{sh}/E_{sol} = 0$, $v_{sh} = v_{sol} = 0.5$. Below the curves the ratio T_p/T_Ω is less than 2 and a dynamic response is probable—above the curves a significant dynamic response is unlikely. As can be seen, even for a rigid impactor, a dynamic response is unlikely unless the impactor is of roughly the same mass or less than that of the fluid-filled shell. The curve obtained by including only the shell stiffness parameter (neglecting the Hertzian contact stiffness) is also plotted and only denoted shell (It is equivalent to the limiting case $\Delta v/c \to \infty$.) It is interesting to note again the significant contribution of the Hertzian contact stiffness even for moderately thin shells.

In Fig. 9 the mass ratio m_{sol}/m_{sh} for which T_p/T_Ω equals 2 is plotted against h/R_{sh} for a number of Young's modulus ratios E_{sh}/E_{sol} ranging from 0 (rigid impactor) to 2. (For this case $\rho_f/\rho_{sh} = 1/2$, $c/\Delta v = 1000$, $v_{sh} = v_{sol} = 0.25$). As would be expected as the stiffness ratio increases the predicted mass ratio to induce a dynamic response also decreases.

4. Conclusions

Analytical expressions have been derived for the response of fluid-filled shells to impact. The analytical model is based on decoupling the Hertzian contact deformation from localized

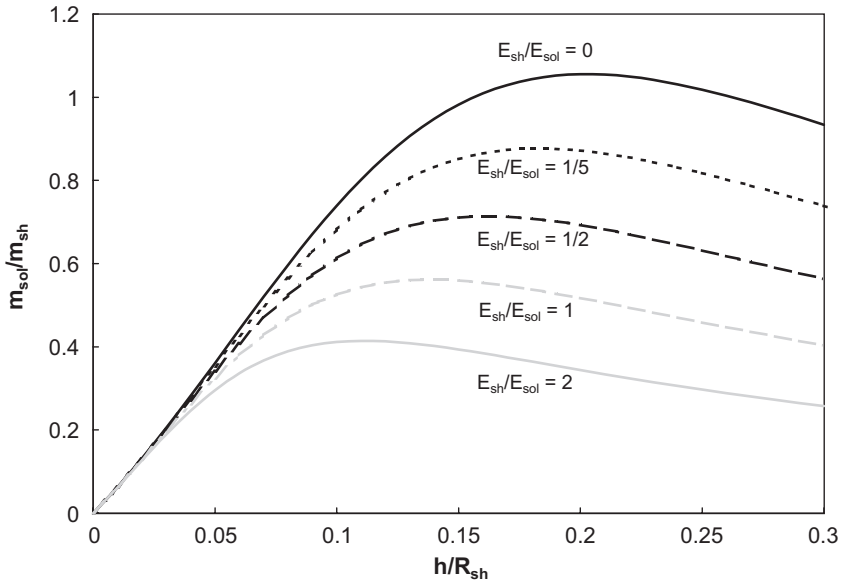

Fig. 9. Non-dimensional mass ratios m_{sh}/m_{sol} delimiting approximate boundaries between quasi-static and dynamic intra-cranial response against thickness ratios h/R_{sh} for a range of non-dimensional stiffness parameters E_{sh}/E_{sol}. (——) $E_{sh}/E_{sol} = 0$; (- - - -) $E_{sh}/E_{sol} = 1/5$; (— — -) $E_{sh}/E_{sol} = 1/2$; (— — —) $E_{sh}/E_{sol} = 1$; (—) $E_{sh}/E_{sol} = 2$.

membrane and bending deformations to provide approximate expressions for key impact parameters including maximum force transmitted, peak acceleration of the shell and duration of impact.

- The proposed analytical model is applicable to fluid-filled shells of arbitrary shell thickness, from very thin shells to solid spheres, subject to constraints defined by the limits of applicability. It should be noted that the usual limits of applicability can be somewhat relaxed if the global impact characteristics, such as the peak force transmitted, are of primary interest as opposed to a more localized characterization of the response, such as the stress or strain field in the vicinity of the impact area.
- The proposed analytical model is applicable to fluid-filled shells and empty shells. In fact, the fluid bulk modulus has no effect on the response and a shell filled with a very low-density incompressible fluid will have the same response as an empty shell. This is true not only of the global impact response but also of the onset of high-pressure transients which is also not a function of the fluid bulk modulus. This point is highly relevant as it explains why both global impact parameters as well as the onset of dynamic effects are not observed to be ostensibly influenced by the presence of a hole, to model the foramen magnum, for example, in numerical and experimental simulations carried out by the author [12,13]. (Although the presence of a hole in the shell will in the quasi-static regime shift the location of the zero pressure nodal point as discussed by a number of authors.)
- Both the Hertzian contact stiffness and the stiffness component from shell bending and membrane action are local effects and therefore the proposed model is applicable to a much

wider range of shell and solid body geometries providing the shell curvatures in the region of the impact are of approximately spherical curvature and constant thickness.

Furthermore, a number of interesting conclusions can be drawn regarding the behaviour of fluid-filled shells to impact:

- For a remarkably wide range of thickness ratios encompassing values typical for the human head, both local shell-membrane and bending deformations and Hertzian contact deformations need to be considered. The use of thin shell theory to model head impacts could therefore lead to significant errors in the predicted response.
- The impact duration drops as the mass of the projectile drops and short impact durations were previously shown to cause very high-pressure transients in the brain. It was here shown that impacts with very heavy objects (e.g., the ground) were unlikely to ever lead to the onset of such large dynamic pressure transients. However, impacts with objects lighter than the fluid-filled shell could cause high-pressure transients to occur; a simple approximate formula (40) was derived to assess the likelihood of a dynamic response of the fluid.
- For a constant impact energy, as the mass projectile drops below a certain threshold the peak pressures observed will increase dramatically, whereas the head injury criterion (*HIC*) will decrease; there is therefore an obvious discrepancy between use of peak pressure (whether positive or negative) as an injury criterion and the *HIC* for impacts with low mass projectiles
- The relative radius of curvature was shown to have relatively little effect on the global response characteristics (although it will obviously have a significant influence on the observed stresses in the contact area).

References

[1] A. Anzelius, The effect of an impact on a spherical liquid mass, Acta Pathologica Microbiologica Scandinavia 48 (1943) 153–159.
[2] W. Guttinger, Der stosseffekt auf eine flussigkeitskugel als grundlage einer physikalischen theorie der entstehung von gehirnverletzungen, Zeitschrift fuer Naturforschung 5 (1950) 622–628.
[3] A.E. Engin, The axi-symmetric response of a fluid-filled spherical shell to a local radial impulse—a model for head injury, Journal of Biomechanics 2 (1969) 325–341.
[4] V.H. Kenner, W. Goldsmith, Dynamic loading of a fluid filled spherical shell, International Journal of Mechanical Science 14 (1972) 557–568.
[5] T.B. Khalil, D.C. Viano, Critical issues in finite element modelling of head impact, Stapp Car Crash Conference, Michigan, USA, 1982, # 821150.
[6] A.A.H.J. Sauren, M.H.A. Claessens, Finite element modelling of head impact: the second decade, Proceedings of the International IRCOBI Conference on the Biomechanics of Impacts, Eindhoven, Netherlands, 1993, pp. 241–254.
[7] L. Voo, S. Kumaresan, F.A. Pintar, N. Yoganandan, A. Sances Jr., Finite-element models of the human head, Medical and Biological Engineering and Computing 34 (1996) 375–381.
[8] J.S. Ruan, T.B. Khalil, A.I. King, Dynamic responses of the human head to impact by 3D FE analysis, Biomechanical Engineering 116 (1) (1994) 44–50.
[9] F.A. Bandak, M.J. Vander Vorst, L.M. Stuhmiller, P.F. Mlakar, W.E. Chilton, J.H. Stuhmiller, An imaging-based computational and experimental study of skull fracture: finite element model development, Journal of Neurotrauma 12 (4) (1995) 679–687.

[10] P.G. Young,C.L. Morfey, Intra-cranial pressure transients caused by head impacts, Proceedings of the 1998 IRCOBI Conference on the Biomechanics of Impact, Gothenburg, Sweden, 1998, pp. 391–403.
[11] P.G. Young, Aparametric study on the axi-symmetric modes of vibration of multi-layered spherical shells with liquid cores of relevance to head impact modelling, Journal of Sound and Vibration 256 (4) (2002) 665–680.
[12] P.G. Young, Finite element corroboration of an analytical model to predict the response of the human head to impact, Presented at the Fifth International Symposium on Computer Methods in Biomechanics and Biomedical Engineering—BioRome Meeting, Rome, Italy, 2001.
[13] P.G. Young, S.R. Diaz, Numerical simulation of the response of the human head to impact using a three dimensional finite element model derived from a medical imaging scan. Presented at the Fifth International Symposium Computer Methods in Biomechanics, Biomedical Engineering—BioRome Meeting, Rome, Italy, 2001.
[14] E.A.C. Johnson, P.G. Young, Response of the human head to impact-an experimental procedure. Presented at the Advanced School and Workshop on: Bone Mechanics, Instituto Superior Técnico, Lisbon, Portugal, 2002.
[15] H. Hertz, Uber Die Beruhrung Fester Elastischer Korper, Zeitschrift fuer die Reine und Angewandte Mathematik 92 (1882) 156–171.
[16] E. Reissner, Stresses and small displacements of shallow spherical shells, II. Journal of Mathematics and Physics 25 (1947) 279–300.
[17] H. Deresiewicz, Anote on Hertz impact, Acta Mechanica 6 (1968) 110.
[18] R.E. Apfel, C.K. Holland, Gauging the likelihood of cavitation from short pulse, low duty cycle diagnostic ultrasound, Ulrasonic Medical Biology 17 (1991) 179–185.